Journal of Volcanology and Geothermal Research 271 (2014) 11–23

Contents lists available at ScienceDirect

Journal of Volcanology and Geothermal Research

journal homepage: www.elsevier.com/locate/jvolgeores

Geodetic observations and modeling of time-varying deformation at Taal Volcano, Philippines

Gerald A. Galgana [a,b,*], Andrew V. Newman [c], Michael W. Hamburger [a], Renato U. Solidum [d]

[a] Department of Geological Sciences, Indiana University, Bloomington, IN 47405, United States
[b] Lunar and Planetary Institute (USRA), Houston TX 77058, United States
[c] School of Earth and Atmospheric Sciences, Georgia Institute of Technology, Atlanta, GA 30332, United States
[d] Philippine Institute of Volcanology and Seismology, Diliman, Quezon City 1101, Philippines

ARTICLE INFO

Article history:
Received 15 May 2013
Accepted 6 November 2013
Available online 1 December 2013

Keywords:
Volcano geodesy
Crustal deformation
Magma chambers
Finite element analysis
Philippines

ABSTRACT

We investigate active crustal deformation patterns associated with magmatic activity at Taal Volcano, an active tholeiitic volcano located in southwestern Luzon, Philippines. We present comparisons of elastic and combined elastic–viscoelastic modeling results with deformation observed by continuous GPS measurements on and near the volcano. Continuous dual-frequency and single-frequency (L1) GPS data between 1998 and 2005 provide evidence for smoothly transitioning periods of inflation and deflation centered under the volcano. Within deformation phases that typically last 3–9 months (with rates exceeding 200 mm yr^{-1}), prominent inflationary phases were observed in February–November 2000 and June 2004–March 2005. The 2000 period of inflation was characterized by up to 145 mm yr^{-1} surface extension and 220 mm yr^{-1} of uplift of the center of Volcano Island relative to the northern caldera rim, while the 2005 inflation was characterized by as much as 116 mm yr^{-1} horizontal extension of the volcanic edifice and 180 mm yr^{-1} uplift. Inversions of observed surface deformation to determine the source location points to a relatively stable spherical source, situated under Volcano Island's central crater, at depths of ~5 km (based on the preferred Mogi model). Using this source geometry, we develop axisymmetric finite element models with annuli of concentric shells around the magma reservoir, embedded within a multi-layered elastic lithosphere. Using simply varying pressure histories as input, a variety of forward models are fit to the time history of continuously observed deformation for GPS stations located on Volcano Island. Though the inferred source geometry, volume and near-source rheological properties are non-unique, they represent more physically appropriate material properties than those assumed in simple elastic half-space models. The sources inferred using viscoelastic shell models suggest simpler pressure histories and reduced overall pressure changes, relative to equivalent elastic half-space models.

1. Introduction

Monitoring time-dependent surface deformation processes of volcanic edifices is vital in estimating magma chamber pressurization and in assessing their volcanic eruption potential. A combination of eruptive and non-eruptive studies is needed to better understand the time-varying processes associated with magmatic storage, ascent, surface extension and eruption. Precise GPS surface position measurements provide a powerful constraint on models of volcanic deformation (e.g., Dzurisin, 2003; Poland et al., 2006). Observed surface motions can be used to infer magmatic deformation at depth, using certain assumptions on the geometry of the source (e.g., Mogi, 1958; Davis, 1986; McTigue, 1987; Yang et al., 1988; Tiampo et al., 2000). Recently, more sophisticated numerical models use material property information to provide an accurate physical representation of the volcanic half-space (e.g., Newman et al., 2001; Trasatti et al., 2003, 2005; Newman et al., 2006; Manconi et al., 2007; Del Negro et al., 2009; Manconi et al., 2010). Here, we use GPS-derived station velocities to locate the magmatic deformation source at Taal Volcano and to constrain numerical models that represent time-varying deformation of its edifice. Using finite-element models of surface deformation, we demonstrate that replacing assumed elastic half-space models with more realistic rheological models of Earth's crust significantly modifies estimates of both the magnitude and the temporal evolution of magmatic source pressure changes. Understanding the nature of strain patterns at actively deforming volcanic systems is critical to making accurate interpretations of surficial changes as related to their eruption potential.

Taal Volcano, situated in the southwestern part of Luzon (the northern and largest island of the Philippine archipelago), is one of the most active of the Philippines' 50 active and potentially active volcanoes, including a number of highly destructive eruptions in the last century (Torres et al., 1995). The volcano is situated within the Macolod Corridor (Figs. 1 and 2), a complex region marking the transition from

* Corresponding author at: AIR Worldwide, 131 Dartmouth St., Boston, MA 02116. Tel.: +1 617 267 6645; fax: +1 617 267 8284.
E-mail address: galgana@lpi.usra.edu (G.A. Galgana).

0377-0273/$ – see front matter © 2013 Elsevier B.V. All rights reserved.
http://dx.doi.org/10.1016/j.jvolgeores.2013.11.005

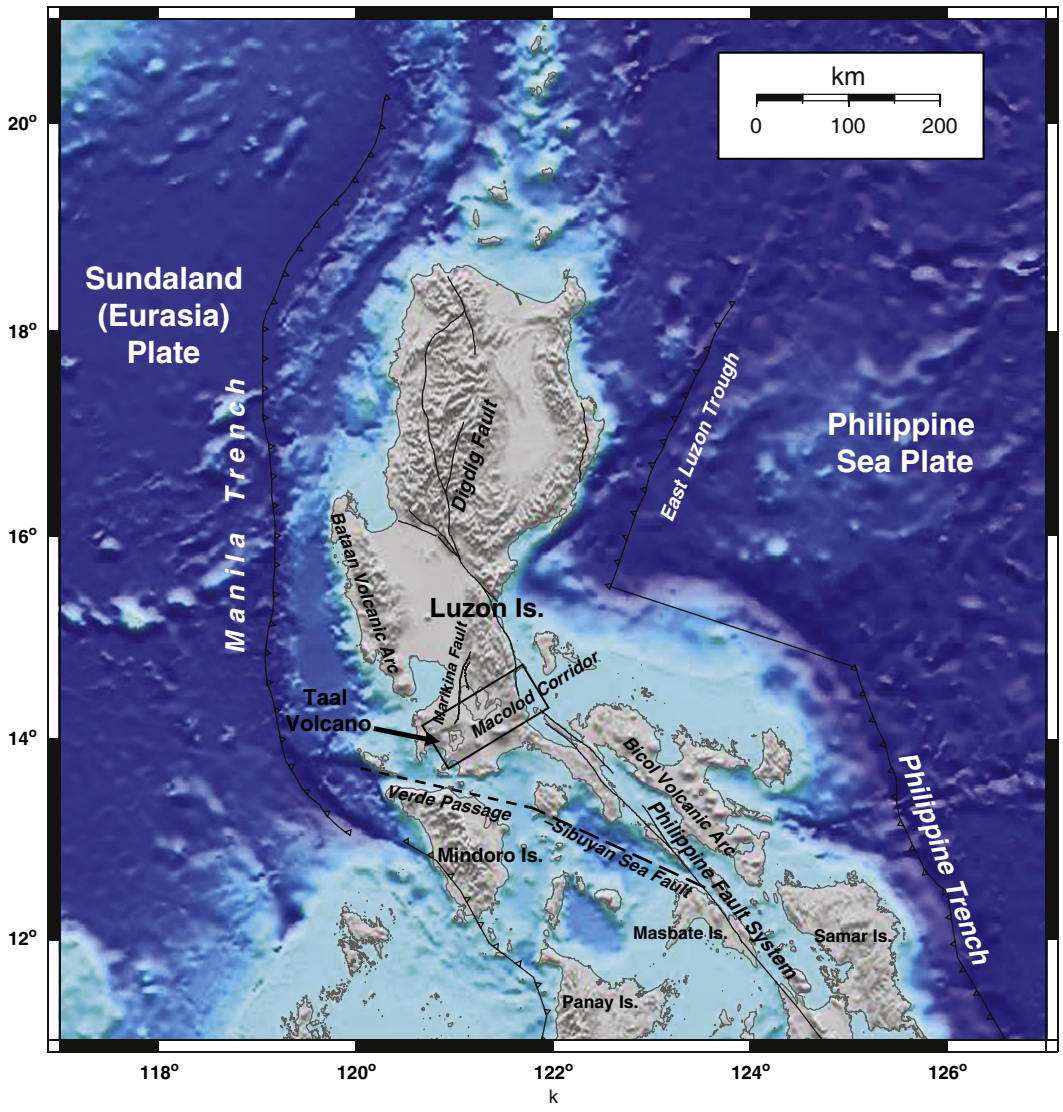

Fig. 1. Map of Luzon, northern Philippines. Major tectonic structures are shown, as well as the major volcanic arcs. Rectangle shows the location of the Macolod Corridor and Taal Volcano region (see Fig. 2). The PMB is bounded on the East by the Philippine Sea Plate, which subducts westward along the Philippine Trench/East Luzon Trough in eastern Luzon, and bounded on the West by the Sundaland (part of Eurasia) block which subducts eastward along the Manila Trench offshore western Luzon. Within the central PMB lies an active sinistral strike-slip fault system, the Philippine Fault, which is responsible for numerous intra-arc earthquakes in the region (Fitch, 1972; Barrier et al., 1991; Aurelio, 2000).

the west-facing Bataan arc in western Luzon to the east-facing Bicol arc in southeastern Luzon (Wolfe and Self, 1982; Torres et al., 1995; Galgana et al., 2007). The zone is characterized by active volcanism, crustal thinning, extensive faulting and block rotations (Förster et al., 1990; Besana et al., 1995; Pubellier et al., 2000; Ohkura et al., 2001; Galgana et al., 2007). Several quaternary volcanoes dot the area; among the more prominent are large volcanic edifices, maars, volcanic craters and exposed dikes (Förster et al., 1990; Torres et al., 1995).

Most volcanoes in western Luzon are silicic in nature, due possibly to terrigenous materials from the subducted slab being incorporated into the melt (Miklius et al., 1991; Mukasa et al., 1994). However, the nature of volcanism in southwestern Luzon is far more varied; basalts, andesites, and dacites have been found in the Quaternary volcanic deposits of the region (Miklius et al., 1991; Oles et al., 1991; Castillo and Newhall, 2004; Vogel et al., 2006). Taal Volcano is located inside Taal Lake, a large fresh-water basin set within a 30 × 25 kilometer-wide caldera (Fig. 2). The main volcanic center is located in a five-kilometer diameter island with 200-meter peaks, characterized by a large central crater (radius ~1 km), flanked by relatively smaller vents. The caldera wall in the north is defined by approximately 700 m of topographic relief at its maximum, and by lower sections in the east and west, with several topographic peaks present in the southeastern region (Torres et al., 1995). The volcano has a history of violent eruptions, ranging from phreatic to violent pyroclastic eruptions. The most recent ones include the 1911 eruption (Volcanic Explosivity Index or VEI = 3), which resulted in widespread devastation within the inner caldera region, and the 1965 eruption, a phreato-magmatic event (VEI = 4) (Moore et al., 1966). Since 1965, the volcano has been associated with repeated volcanic crises, which have led to several evacuations of Volcano Island (Bartel et al., 2003; Zlotnicki et al., 2009).

Taal Volcano has an extensive history of GPS deformation studies on which the current research is built. Campaign-based GPS measurements began there in 1996 (Thibault, 1999), followed by establishment of the continuous volcano-monitoring GPS networks described here in 1998. Lowry et al. (2001) presented analysis of the dual-frequency network data for the period 1998–2000; Bartel et al. (2003) analyzed data from the dual- and single-frequency GPS networks for the period 1999 to 2002. Initial measurements of volcano deformation, based on the dual-frequency GPS network in 1998 and 1999 (Lowry et al., 2001), revealed as much as 150 mm yr^{-1} change in horizontal velocities,

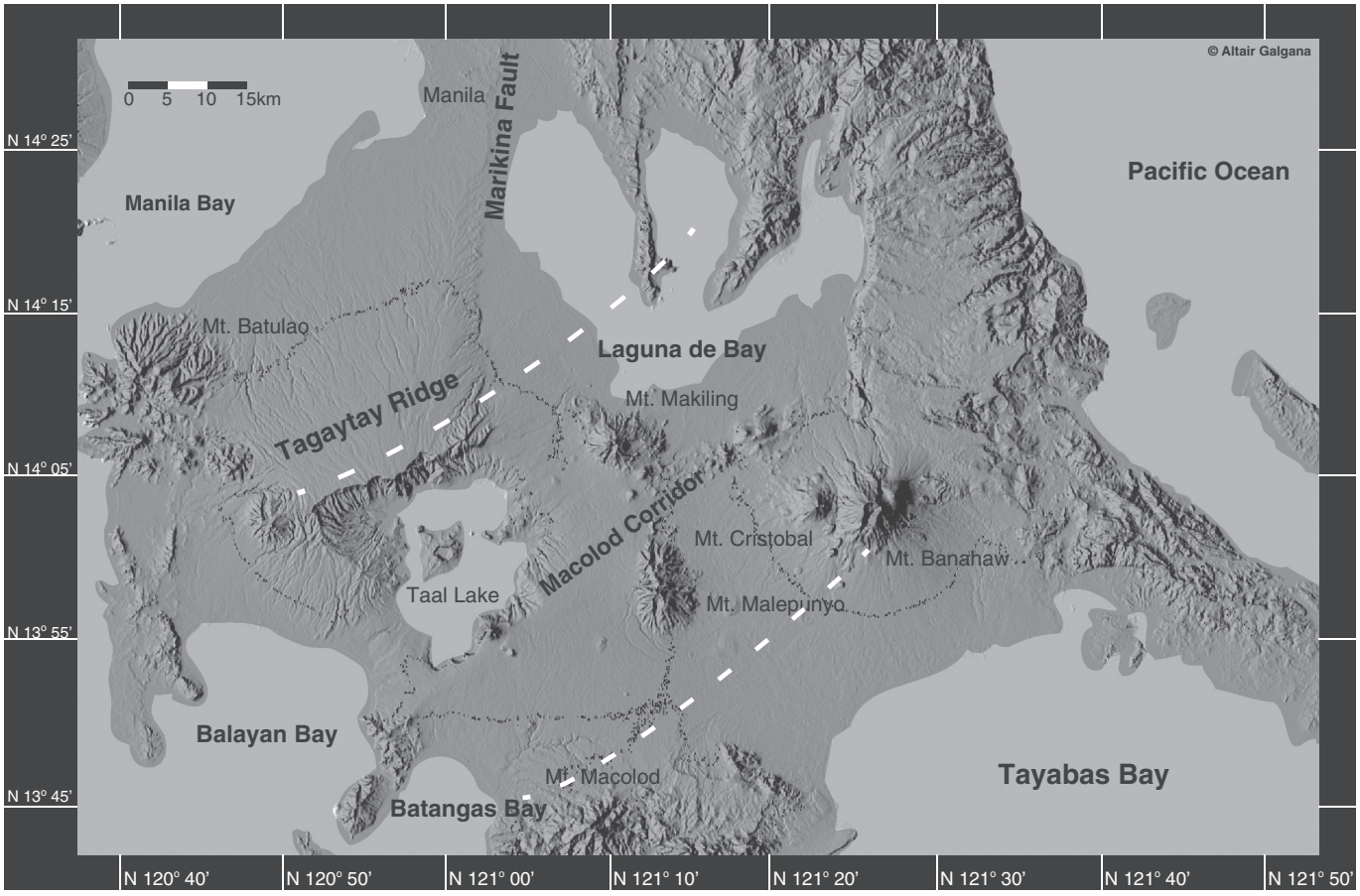

Fig. 2. Physiographic map of the Macolod Corridor area. Major volcanic centers, tectonic faults and dike systems are shown. Taal Caldera is situated on the western part of the corridor.

with the source of inflation determined to be localized around Volcano Island. Subsequently, using the present combination of single- and dual-frequency GPS stations, Bartel et al. (2003) measured as much as 120 mm uplift of the volcano edifice in 2000, with average vertical rates of ~216 mm yr^{-1}. They also determined the locations of inferred point sources of deflation and inflation at Taal during 1999 and 2000 to be located beneath Volcano Island's main crater at depths of 4.2 and 5.2 km, respectively. This study builds on these previous GPS investigations by extending the observational base through 2005 and enhancing the geodynamic analysis using anelastic rheologies to better constrain the behavior of the magmatic source beneath Taal.

2. Continuous GPS data acquisition and processing

Volcano deformation at Taal has been monitored by two, complementary GPS networks: a three-station dual-frequency network in and around Taal Volcano from 1998 to 2005, and a network of 11 single-frequency (L1 GPS) stations distributed around the volcano and the caldera rim (Lowry et al., 2001; Bartel et al., 2003), from the period 1999 to 2005 (Figs. 3–4, Table 1). These dual- and single-frequency L1 data are processed using the Bernese GPS Software Version 4.2 (Rothacher and Mervart, 1996; Hugentobler et al., 2001). Dual-frequency station data are processed along with data from two fiducial stations in Manila, MMA8 and PIMO. Baselines for both dual- and single-frequency stations are determined relative to station KAYT, which has the most extensive temporal period of observations. GPS data are processed using multiple steps involving cycle-slip filtering, removal of outliers, estimation of tropospheric parameters, ambiguity resolution, and determination of a network-wide solution for daily positions and covariances of the GPS sites (Lowry et al., 2001). L1 data accuracy is increased by using a global ionosphere model (GIM) from the Center for Orbit Determination (CODE, a part of the International Global Navigation Satellite System Service (IGS)) to estimate delay parameters from the L1 GPS data. These L1 corrections are applied in the final coordinate solution. Details of the processing are fully described in Bartel (2002). In this research, we extend the temporal range of the observations by including dual-frequency data from 2001 to 2005, as well as 2004–2005 data from the single-frequency stations. The data were recorded for the Taal network through July 2005, when data transmission stopped (permanently) due to the failure of the telemetry system.

2.1. Observed deformation patterns

During the monitoring period, alternating episodes of volcanic deflation (September–November 1998, May–October 1999) and inflation (January–March 1999 and February–October 2000) were observed (Fig. 3). These periods can be readily identified from the changing slopes of the three components within the displacement time series (Fig. 4). For these particular station configurations, positive slope indicates inflation, while negative slope indicates deflation. Similarly, map view patterns of the station horizontal velocity vectors readily indicate inflation (velocity arrows pointing radially outward) or deflation (arrows pointing radially inward). Such periods were interpreted to be associated with magma upwelling and depletion events, characterized by a relatively static source location, as determined by point-source inversions implemented using a time-varying window (Bartel et al., 2003).

The year 2000 inflationary period resulted in as much as 145 mm yr^{-1} horizontal lengthening of the volcanic edifice (i.e., measured though baselines TVST-KAYT and TV05-KAYT), with ~220 mm yr^{-1} maximum uplift rates with respect to the caldera rim,

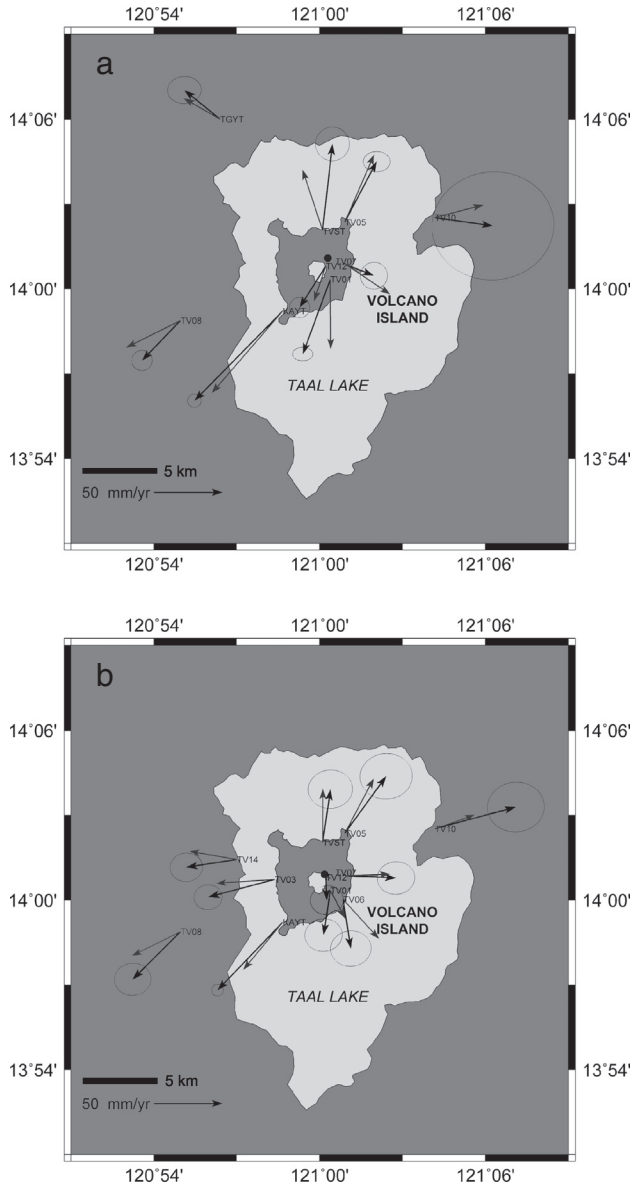

Fig. 3. Map of observed (black arrows with 95% confidence ellipses) and predicted (gray arrows) GPS velocities of stations in Taal Volcano for the (a) March–October 2000 inflationary period (Modified from Bartel et al., 2003); and (b) the January–February 2005 inflationary period. Overall pattern of velocity vectors in both cases are consistent with those produced by a radially expanding Mogi point source situated near the center of Volcano Island.

measured through the baseline TV12-TGYT. In contrast, the 1999 deflationary event resulted in as much as 40 mm yr^{-1} horizontal shortening across the volcanic edifice, with vertical subsidence rates of about 30 mm yr^{-1} with respect to the caldera rim (Bartel et al., 2003). We also observe a prominent inflationary trend which started in June 2004, which continued through January 2005 and peaked near the end of February 2005 (Fig. 4). This inflationary trend changed to deflation by March 2005, and progressed with variable signal until July 2005 when the last data was recorded. This event resulted in as much as 116 mm yr^{-1} horizontal extension across the volcanic edifice (measured through stations KAYT and TV05), and uplift rates of as much as 180 mm yr^{-1} with respect to the caldera rim (e.g., TV01 with respect to TGYT). For our analysis, we focus on the observed inflationary trend in January–February 2005, which was characterized by high-quality observations, less data scatter and a steeper, constant inflationary signal (Fig. 4). This early 2005 inflationary event coincided with a higher number of volcanic tremors, observed from a network of short-period seismographs near the volcano (*J. Sabit, Pers. comm.*, 2006; Zlotnicki et al., 2009).

3. Volcano deformation models

We analyze recent deformation of Taal Volcano in two steps: first, we determine the location of the magmatic source for the 2004–2005 rapid inflation using an elastic point-source 'Mogi model' inversion (Mogi, 1958; Dzurisin, 2003); second, we construct a finite element model of the magmatic source region in order to refine estimates of time-varying surface deformation and magmatic source pressurization. The inferred depth of the magma chamber is based on the Mogi source depth as determined in step 1, with the shape assumed to be a simple sphere with the radius based on geologic estimates. We note that the analytical point source model considers a spherical magmatic source whose size is small relative to its depth. The approach is insensitive to initial source volume and is used to determine temporal changes in source pressure and, by inference, changes in source volume (Lisowski, 2006). In step 2, we fix the position of the magma source geometry and focus on modeling the rheology and time-dependent aspect of pressure change. Rock properties derived from published experimental results, such as Young's, shear, and bulk moduli can be applied to components of the finite element models (e.g., Dieterich and Decker, 1975; Newman et al., 2001; Trasatti et al., 2003, 2005; Newman et al., 2006; Manconi et al., 2007; Del Negro et al., 2009; Manconi et al., 2010).

3.1. Determination of magmatic source location

Because active magmatic systems produce high local deformation rates with respect to the long-term tectonic deformation, we adopt the modeling approach that neglects the slow, long-term tectonic component and instead focuses on abrupt changes at smaller spatial and temporal scales (Dzurisin, 2003). Furthermore, in volcanic settings, it is difficult to isolate deformation signals originating from non-magmatic or hydrothermal sources. Following previous studies at Taal (Lowry et al., 2001; Bartel et al., 2003), we consider that the ongoing volcanic deformation is primarily magmatic in origin: i.e., deformation originates from a single point source (Fig. 5). In common with many volcanic deformation studies (e.g., Dvorak and Dzurisin, 1997), we assume a simple (spherical) source geometry, since a more complicated source structure has not been indicated by the spatial characteristics of the geodetic signal, and because the density of GPS observations in our network appears to be insufficient to uniquely characterize such geometries. The pattern of seismicity near Taal volcano during the period 2005–2006 (*J. Sabit, pers. comm. 2006*; Zlotnicki et al., 2009) also indicates a relatively localized source of deformation beneath Volcano Island. To determine the source location, we initially select subsets of the dual-frequency data which represent a steady, unambiguous increase or decrease in slope (i.e., those representing systematic change in position for a period greater than 1 month). Then, the combined time series data (the three dual-frequency GPS stations and the 12 single-frequency GPS stations) are used as input to the point-source modeling process. We use DisModel, the MATLAB-based inversion program (Cervelli et al., 2001) that implements a Levenberg–Marquardt constrained least-squares inversion to arrive at the best-fit Mogi source based on surface velocities or displacements. We then use this Mogi source location as the center of the spherical magma chamber to construct the finite element model used in stage 2.

3.2. Finite element models

Because assumptions about crustal rheology can have a significant impact on inferred magmatic source properties, we investigate forward models of magmatic sources embedded in media that differ from the

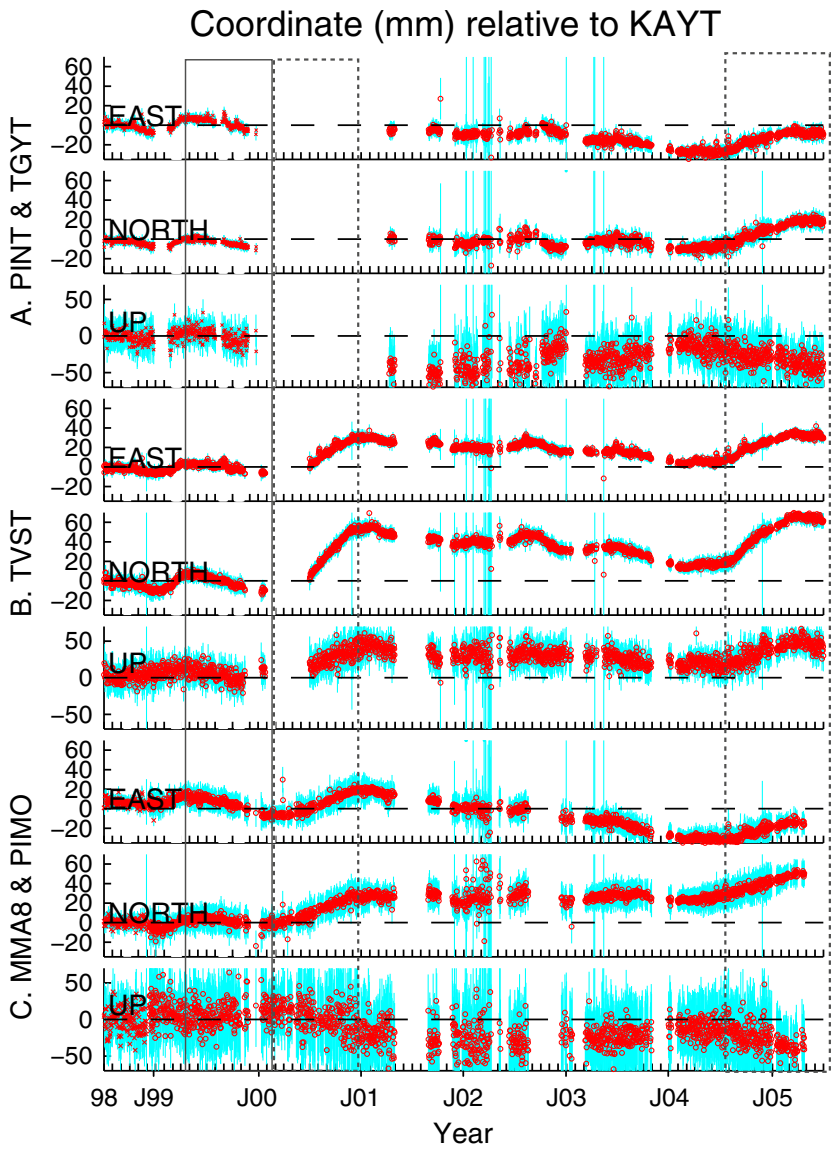

Fig. 4. Time series of dual-frequency GPS stations (coordinates in mm with respect to KAYT) from June 1998 to July 2005. Alternating periods of inflation and deflation are reflected by the time series data, by plots that show East, North, and vertical coordinate component change for stations (A) TVST (1998–2005), (B) PINT (1998–2000)/TGYT (2001–2005), and (C) MMA8 (crosses, June to November 1998)/PIMO (1998 to 2005). Red circles and crosses represent positions, while vertical bars (cyan) depict are 95% errors scaled to repeatability. PIMO and MMA8 are dual-frequency stations situated in Manila, ~30 km north of the Caldera, while PINT was formerly the GPS station situated at the present location of TV07. Boxes indicate the deflationary (box with thin solid line) and inflationary periods (boxes with dashed lines) under study. (For interpretation of the references to color in this figure legend, the reader is referred to the web version of this article.)

traditional elastic half-space assumption. In our experiments, we consider the viscoelastic (VE) nature of low temperature magma and country rock surrounding the magma chamber as well as the varying rigidities of horizontally layered regions of the surrounding crust. Magmatic sources in long-lived volcanic systems (particularly in silicic volcanoes where the temperature difference between rocks near the magma chambers are more subtle) are best represented with heterogeneous rheologies (Fig. 6, Table 2). In such settings, high temperatures near the magma body tend to create a region where the crust behaves more like a viscoelastic material (Dragoni and Magnanensi, 1989; Newman et al., 2001; Trasatti et al., 2005). Rocks near the magma source may behave as a Maxwell viscoelastic fluid (i.e., represented as spring and dashpot in series), rather than a simple elastic solid (Newman et al., 2006). To incorporate this rheology, finite elements have been used in the past to model complex crustal regions near volcanic centers (e.g., Dieterich and Decker, 1975; Manconi

Table 1
Observed horizontal and vertical velocities of GPS stations with respect to station KAYT, for the January–February 2005 inflationary event. Coordinates are in degrees, while velocities and sigma values are in mm yr^{-1}.

STA	Long	Lat	Ve	Vn	Vz	σE	σN	σZ	E-N Corr.
TV01	121.0064	14.0055	43.80	14.69	15.68	10.52	9.19	2.05	0.0190
TV03	120.9729	14.012	−3.91	35.05	−0.04	7.90	7.02	1.56	0.0136
TV05	121.0152	14.0391	77.47	86.19	2.77	14.81	12.95	2.90	0.0155
TV06	121.0143	14.0004	52.59	11.62	11.91	11.48	10.05	2.24	0.0197
TV07	121.016	14.0142	81.88	45.39	14.44	10.52	9.19	2.06	0.0188
TV08	120.9161	13.9814	15.79	14.78	0.20	10.35	9.20	2.04	0.0161
TV10	121.0695	14.0419	84.70	57.24	−8.93	15.88	13.85	3.10	0.0155
TV12	121.0037	14.0134	47.58	30.74	8.94	9.30	8.18	1.82	0.0167
TV14	120.9502	14.0238	13.24	40.71	1.74	9.19	8.16	1.81	0.0155
TVST	121.0018	14.034	52.91	84.11	11.53	12.52	10.88	2.44	0.0172
TGYT	120.9385	14.1008	34.79	92.28	−2.02	13.40	11.94	0.90	0.0314

et al., 2007, 2010). This approach offers a reasonable alternative to analytical techniques (i.e., Dragoni and Magnanensi, 1989), particularly in areas where complicated changes in material properties are suspected.

3.3. Model setup

To accurately model time-varying crustal deformation around Taal volcano, we ran a series of numerical simulations using finite element models designed with ABAQUS software (Hibbit, Karlson, Sorenson, Inc., 1998; ABAQUS, 2003). Using this approach, however, some simplifications were made to accommodate the limitations of the software: gravitational effects are ignored, surface topography is considered flat, and the magmatic source is constrained to be a simple, stationary (temporally non-migrating) sphere. We did not model gravitational loading to avoid complications associated with material responses near the boundary, while topographic effects are small in areas of low elevation (e.g., Trasatti et al., 2005). Given that the edifice height of Taal Volcano is less than 200 m from base to summit, we expect that variations introduced by topographic offsets are sufficiently low. Furthermore, Newman et al. (2001) noted insignificant differences between the deformation patterns predicted by analytical and numerical (elastic) full space solutions, based on their studies at Long Valley caldera.

We represent the immediate region around Taal Volcano as an axisymmetric solid section with dimensions of 50 km radius and 50 km depth, represented by approximately 13,000 quadrilateral finite elements (Fig. 7). We selected these model dimensions to be sufficient to avoid edge-related effects, and treated the rheology of the lower crust to be elastic. The crustal layers around Taal volcano are represented by three horizontal, elastic layers that represent shallow, intermediate, and deep crustal strata. The intermediate layer is composed of an inner and outer region representing the transitional and distal intermediate regions from the magma chamber; a lower layer with higher elastic rigidity represents the lower crust (Fig. 6). We assign an elastic rigidity of $\mu = 5$ GPa (typical crustal values for volcanic areas based on Bonafede et al. (1986) for the two upper layers), including the transition zone and $\mu = 30$ GPa for the bottom layer representing strong basement rock (Masters and Shearer, 1995). We use a Poisson's ratio (ν) of 0.25 for all the layers (Table 2).

The magma chamber is represented by a 1-kilometer radius sphere with the center embedded at 5 km depth. The radius is approximately equal to the radius of the central volcano crater, which may roughly represent the outer extent of the magma chamber (e.g., Roche et al., 2000; Cole et al., 2005). The immediate rock walls surrounding the magma chamber are modeled as 500-meter thick, concentric spheres with progressively increasing viscosities, i.e., rock becomes more viscous (lower temperature) as the distance from the center of the magma chamber increases, corresponding to temperature-dependent rigidities of rocks surrounding the magma chamber (Fig. 6). The overall thickness of the concentric shells is maintained to be 1.5 km, corresponding to average thicknesses of eroded remnants of magma chamber walls observed on the field, as reported in Newman et al. (2001). The top of the model is treated as a free surface. To isolate extraneous movements along the model boundaries, lateral motion and vertical motion are constrained along the outermost and bottom boundaries of the model, respectively. A pattern of distributed normal stress representing constant overpressure is imposed along the reservoir wall to simulate the influx and outflux of magmatic material. When no pressure is applied, the system is in equilibrium, since no internal deformation due to gravity, tectonic stress and other external loads are imposed.

In separate model runs, we represent the surrounding shells around Taal's magma chamber with three different rheologies: first, composed of purely elastic material, approximating the analytical point-source solution; second, with the inner shells composed of highly viscous material; finally, we use a material with lower viscosity for the inner shells. The second configuration reflects the expected material properties of felsic (rhyolitic) material corresponding to the caldera-forming eruption layers of Taal Volcano, which corresponds to an elastic rigidity of $\mu = 5$ GPa and viscosities of 10^{17} to 10^{18} Pa-s (Richet et al., 1996; Ivins, 2000). The third configuration uses the same rigidity values as the second, but with significantly lower viscosities of 10^{13} to

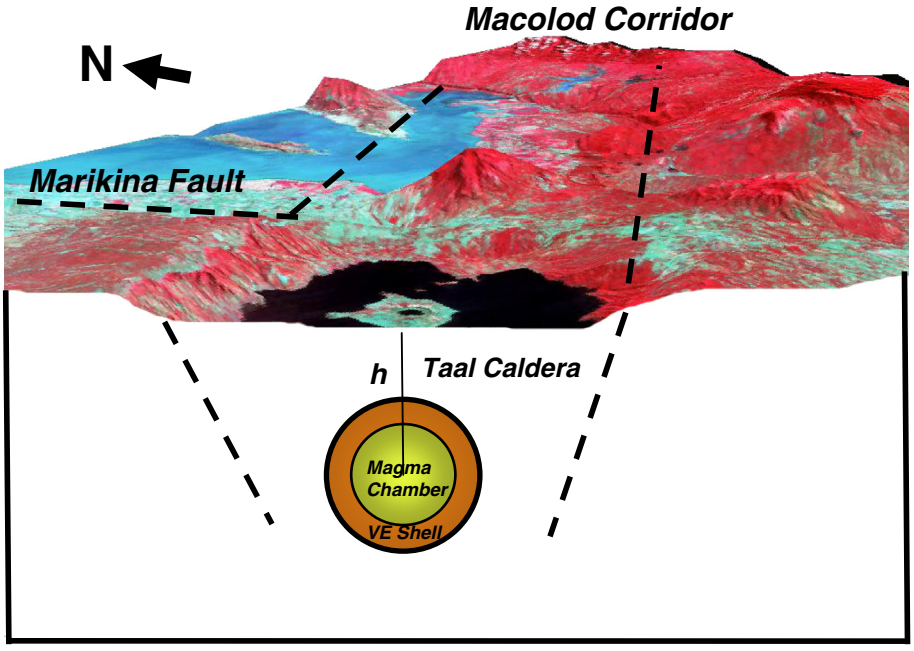

Fig. 5. Hypothetical cross section of Taal Volcano and the Macolod Corridor (processed Landsat data over DEM, plotted not to scale).

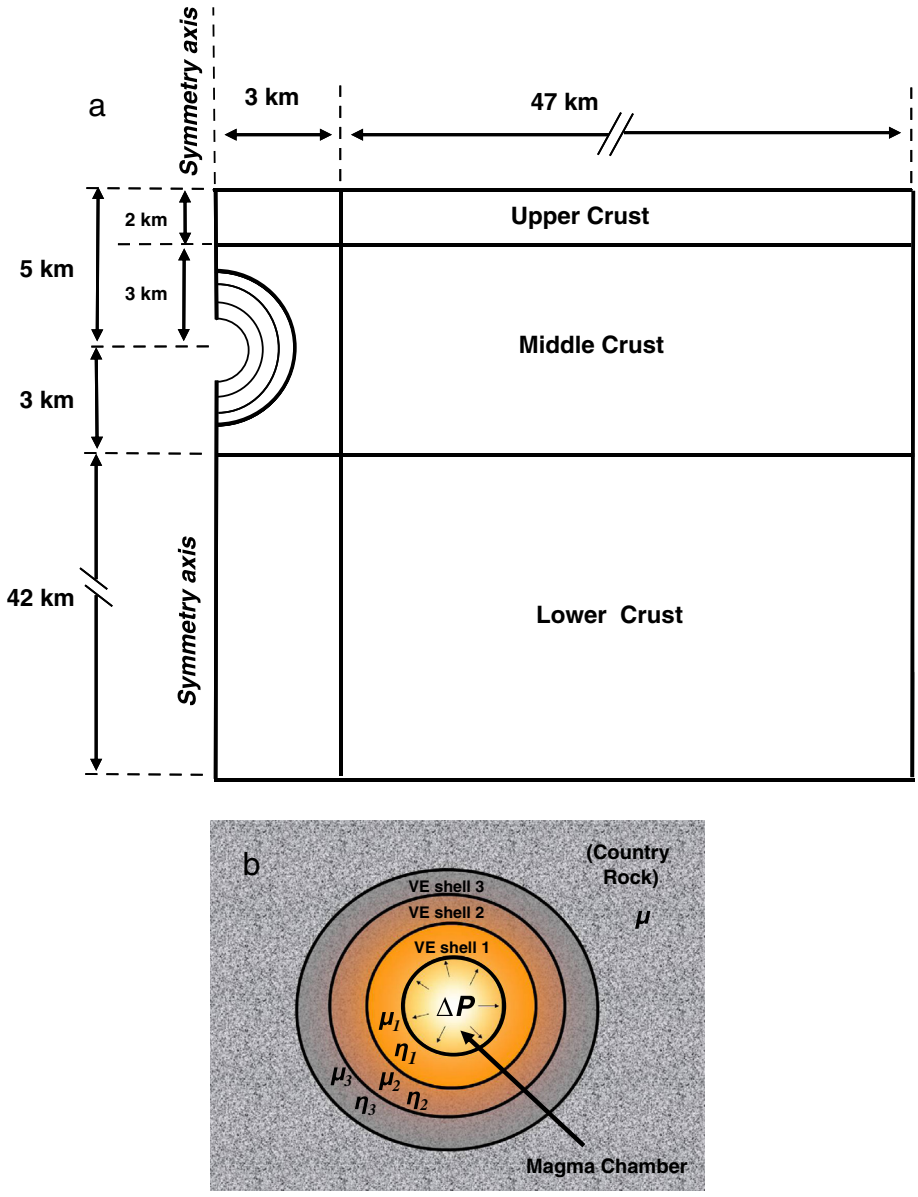

Fig. 6. Taal model setup. Fig. 6a shows axisymmetric model, with different layers of the crust and regions near the magma chamber. Fig. 6b shows spherical magma chamber with concentric shells with different material viscosities. Rheological parameters are summarized in Table 2.

10^{15} Pa-s. These values correspond to the rheology of andesites at temperatures 610 °C to 670 °C with 1-5% H_2O by weight percent, assumed to be about 40–60% crystallized by volume. The magma viscosities are derived using empirical techniques (i.e., Shaw, 1972; McBirney and Murase, 1984) implemented through K-Ware Magma (Wohletz, 1999).

Table 2
Material property constants used for various layers and components of the finite element models. The relaxation times are based on Maxwell viscous material responses, while values inside parentheses report values corresponding to the geometry-dependent VE shell relaxation formula of Bonafede et al. (1986).

Model layer/shell	Elastic parameters			High-viscosity model		Low viscosity model	
	Young's modulus (E)	Rigidity (μ)	Poisson's ratio (ν)	Relaxation time (τ)	Viscosity (η)	Relaxation time (τ)	Viscosity (η)
Inner VE Shell	12.5 GPa	5 GPa	0.25	23.15 d (140.6 d)	10^{16} Pa-s	0.02 d (0.14 d)	10^{13} Pa-s
Middle VE Shell	12.5	5	0.25	231.5 d (987.7 d)	10^{17} Pa-s	0.23 (0.99 d)	10^{14} Pa-s
Outer VE Shell	12.5	5	0.25	2314.80 (8138 d)	10^{18} Pa-s	2.32 (8.14 d)	10^{15} Pa-s
Mid, Transitional	12.5	5	0.25	–	–	–	–
Shallow Crust	12.5	5	0.25	–	–	–	–
Middle Crust	12.5	5	0.25	–	–	–	–
Deep Crust	75	30	0.25	–	–	–	–

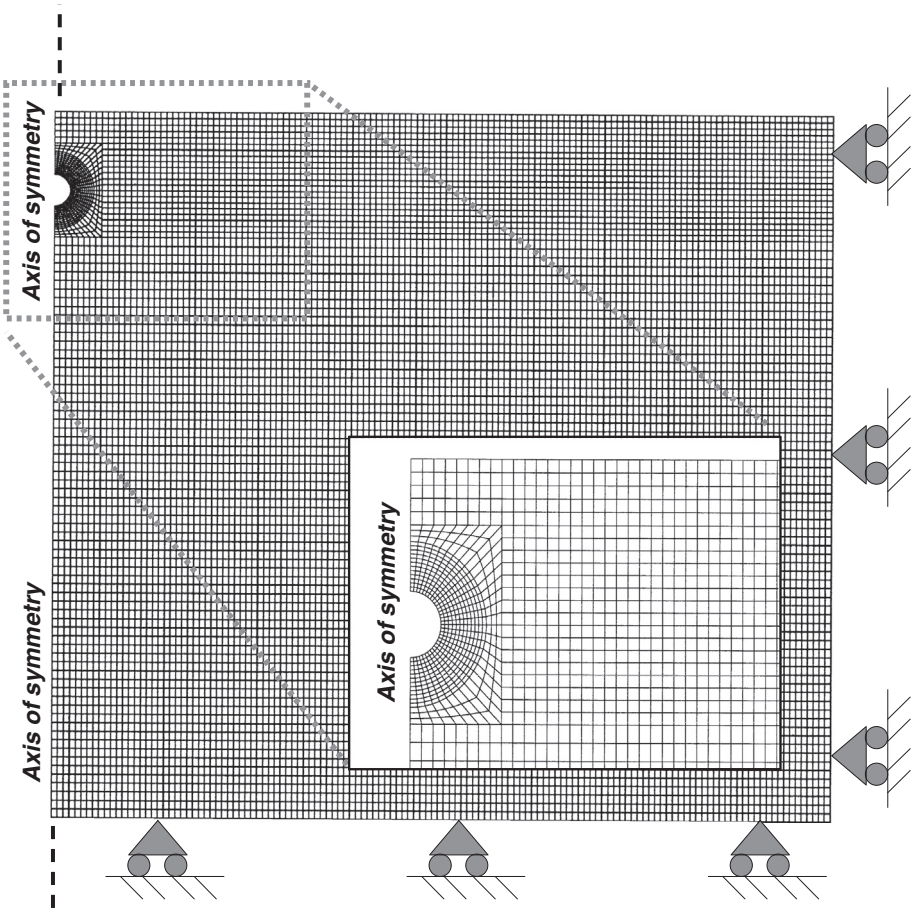

Fig. 7. Finite element mesh and model boundary conditions. The 50 km radius by 50 km thick axisymmetric model is composed of approximately 13,000 quadrilateral elements with higher resolution within the shallow layers, and increasing toward the magma chamber wall. Roller boundary conditions are applied at the bottom and the distal part of the model, with normal stresses applied along the magma chamber wall to simulate magma pressurization. Inset near the center of the mesh zooms to the magma chamber part of the undeformed model.

3.4. Tests for data-model agreement

The forward modeling process starts when initial perturbations (i.e., pressure pulses at specific points in the deformation time series) are applied normal to the magma chamber wall. These pulses translate to contact stresses and in turn, strain in the intervening shells and crustal layers, eventually resulting in surface deformation of the axisymmetric model. Time-dependent surface displacements at any location in the model can be derived. The resulting deformation for selected sites or at specified coordinates (predicted displacement) is then matched to the observed station data (observed horizontal and vertical components of deformation). Comparisons between the model and the observed data can be quantified using the total chi-square (χ^2) and the reduced chi-square tests (e.g., Press et al., 1992; Newman et al., 2006). Thus we attempt to find a good data-model fit by minimizing the reduced chi-square values for all three components of surface deformation (i.e., *E*, *N*, and *Z* velocities).

4. Results

4.1. Mogi source location

The period February to November 2000 shows steady changes in position for most of the stations, unmistakable indicators of volcanic inflation. Based on point-source model inversion, the source of this deformation was determined to be at 14.021°N, 120.999°E, depth = 5.2 km beneath the NE part of Volcano Island (Bartel et al., 2003). Similarly, the period June 2004 to 2005 shows a constant velocity for most of the stations, another indication of volcanic inflation. Similarly, our results from the joint inversion of dual-frequency and single-frequency data for the 2005 inflation episode show that the Mogi source was situated northeast of Crater Lake, at 14.013°N, 121.003°E, at a depth of 5.1 km (Fig. 3, Table 3). This location is near the inflationary source found for the 2000 event, indicating that the magma source is nearly stationary, although secondary, local-scale source migration cannot be ruled out. On the other hand, the 1999 deflationary source is found to be at 13.995°N, 121.017°E, situated south of the inflationary sources, near the south shore of Crater Lake, at a somewhat shallower depth of 4.2 km (Bartel et al., 2003).

Table 3
Inversion results for the Mogi source location based on the 1999–2000 and 2004–2005 events. Inner stations refer to those GPS stations within volcano island.

Event/Reference	Year	Latitude	Longitude	Depth (km)
Deflation (Inner stations)/ Bartel et al. (2003)	1999	13.995°N	121.017°E	4.2
Inflation (Inner stations)/ Bartel et al. (2003)	2000	14.021°N	120.999°E	5.2
Inflation (Inner stations)/ This Study	2005	14.013°N	121.003°E	5.1

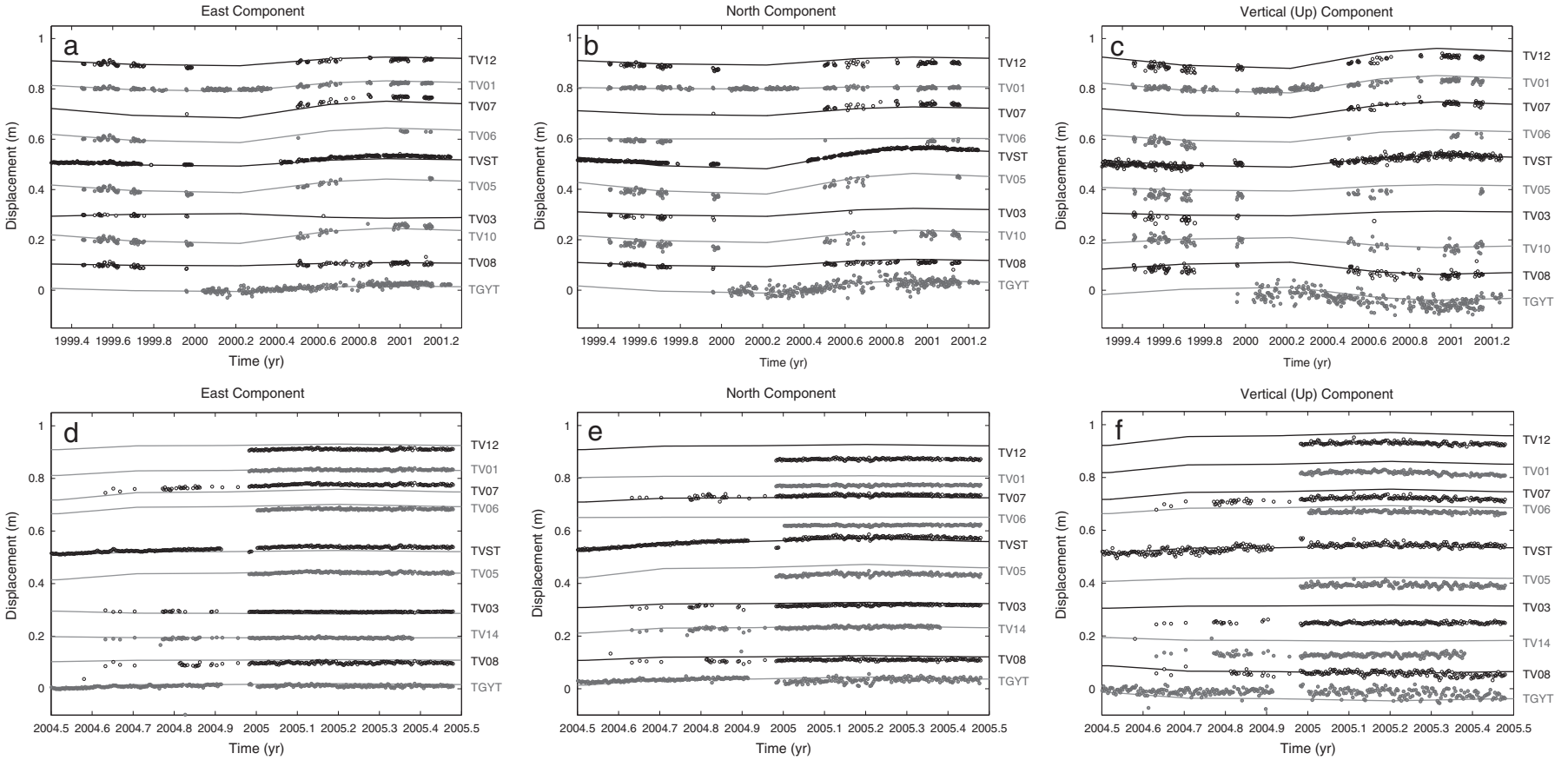

Fig. 8. Plots comparing the modeled surface deformation with observed GPS data. Fig. 8a–c shows the deflation–inflation pattern during the period 1998–2001; Fig. 8d–f shows the 2005 inflation. Note that individual station plots are offset from the origin, 0.1 m from the preceding lower plot.

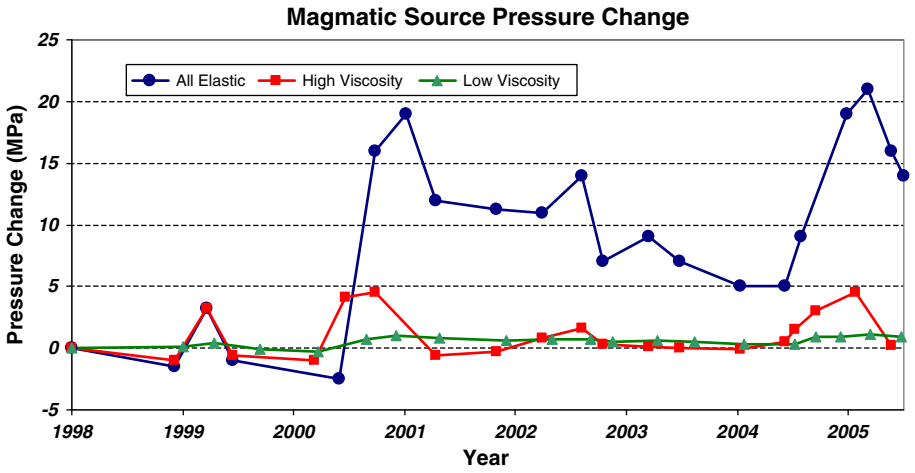

Fig. 9. Pressure histories of the elastic model and two viscoelastic models within the period 1998–2005. The pressurization curves were estimated by fitting the predicted surface deformation (from forward models) to the observed KAYT-TVST GPS baseline data.

4.2. Rheological effects and pressure history estimates

As described above, we examine the volcanic source at Taal using finite elements with three different rheological configurations: (1) a purely elastic shell geometry; (2) shells with high viscosities (i.e., equivalent to rhyolites and dacites); and (3) shells with low viscosities (i.e., andesites). In all three cases, we compare observed deformation (i.e., surface displacements) with the predicted deformation by pressure increases attributed to magma inflation (in 2000, 2002, 2003 and 2004–2005). Notably, there are also pressure dips, presumably associated with magma withdrawal, during the years 1998, 1999–2000, 2001, 2002 and 2005 (Figs. 4, 8–9). Since the models we use are axisymmetric, the predicted displacements are all symmetric to the model origin (and may not fully match the observed deformation field due to either to other localized sources or to asymmetry in the rheological parameters). The magnitude and temporal distribution of the pressurization pulses, however, vary significantly according to model rheology. While all three models can effectively match the spatial displacements shown by the observed data, the elastic model requires higher pressures (about four times that predicted by the high-viscosity model, and about ten times as much as predicted by the low-viscosity model) to produce the equivalent magnitude of surface deformation. An important distinction between the models is that the elastic model requires instantaneous pressure changes (i.e., from single or progressive pulses) to match each of the observed deformation, while the viscoelastic models permit some temporal lag between pressure pulse and observed deformation. In other words, the two viscoelastic models require slightly earlier pressure pulses (by about 30 days) in order to match the observed pattern of surface deformation. An important implication of this model is that some of the temporal changes in surface deformation can be explained by viscous relaxation, rather than actual magmatic withdrawal (Newman et al., 2001; Manconi et al., 2007; Del Negro et al., 2009). The lower viscosity VE shell model matches the same deformation field using about 20–25% of the pressure change used in the high-viscosity VE shell model (Fig. 9).

To further verify the contribution of individual shells to the total surface deformation, we run separate tests that turn on each shell (i.e., by making them viscoelastic), then we apply a constant, instantaneous pressure on the inner reservoir wall. We then observe the resulting surface displacements arising from varying the number of viscoelastic shells, in effect varying the thickness the viscous zone of rocks around the reservoir. Reducing the number of shells to include only the innermost two shells transmits associated stresses and strains to the surface about ten times faster than the model that includes all three shells. Thus, we find that thicker shells increase the delay factor in surface deformation arising from reservoir pressurization pulses. Furthermore, with similar pressurization, we find larger surface deformation from models with viscoelastic shells compared to those with purely elastic ones (similar to the findings in Long Valley by Newman et al., 2001). Conversely, a smaller pressure change is required to reproduce the observed deformation rates. The effective relaxation times of the VE shells tend to be much longer than their corresponding Maxwell times (see Table 2), primarily due to the overall effect of the VE shell geometries: That is, the resulting individual shell relaxation times would tend to follow the equation

$$\tau = \frac{9\eta}{5\mu}\left(\frac{R_1}{R_2}\right)^3$$

where is τ the relaxation time, μ is the shear modulus, η is the viscosity, R_2 is the outer shell radius, and R_1 is the inner shell radius (Bonafede et al, 1986; Dragoni and Magnanensi, 1989), rather than the relationship described by the relaxation equation, $\tau = \eta/\mu$.

4.3. Data-model agreement

As described above, we first use the dual-frequency stations to constrain surface deformation of the models and determine the time-varying pressurization history. We then compare the predicted deformation time series from the preferred model (in this case, the low viscosity model was preferred due to its rheological similarity with rocks found in the Taal region) with the observed coordinate change time series at every GPS station, including both single- and dual-frequency networks. Table 4 summarizes the dual frequency

Table 4
Data-model fit summary (Chi-square errors) for the dual-frequency stations, based on the entire period of 1998–2005. The 2005 Mogi source location is used to constrain the finite element models. Lines marked with "data" indicate the total number of observations.

Station/Component	1998–2005	
	Total $\lvert\chi^2\rvert$	Reduced $\lvert\chi^2\rvert$
TVST-E	1832	1.23
TVST-N	853	0.57
TVST-Z	145	0.10
Data		1500
TV13,TGYT-E	189	0.16
TV13,TGYT-N	593	0.51
TV13, TGYT-Z	348	0.30
Data		1168

Table 5
Data-model fit summary (Chi-Square Errors) for all stations, for the periods 1998–2001 and 2004–2005. Here, the preferred low-viscosity model is compared to the observed GPS data. The 2005 Mogi source location is used to constrain the finite element models.

Station/Component	Radial distance from	1998–2001		2004–2005	
	2005 source	Total $\lvert\chi^2\rvert$	Reduced $\lvert\chi^2\rvert$	Total $\lvert\chi^2\rvert$	Reduced $\lvert\chi^2\rvert$
TV12-E	0.1 km	106	0.96	676	2.79
TV12-N	0.1	273	2.48	1858	7.68
TV12-Z	0.1	145	1.32	752	3.11
Data			124		256
TV01-E	0.9	7	0.03	39	0.24
TV01-N	0.9	15	0.07	710	4.44
TV01-Z	0.9	19	0.09	522	3.26
Data			220		174
TV07-E	1.4	163	3.54	381	2.47
TV07-N	1.4	99	2.15	117	0.76
TV07-Z	1.4	4	0.09	347	2.25
Data			60		168
TV06-E	1.9	34	0.74	255	1.66
TV06-N	1.9	66	1.43	531	3.45
TV06-Z	1.9	52	1.13	235	1.53
Data			60		168
TVST-E	2.3	754	1.17	567	1.15
TVST-N	2.3	131	0.20	304	0.62
TVST-Z	2.3	128	0.20	18	0.04
Data			660		507
TV05-E	3.2	42	0.67	77	0.48
TV05-N	3.2	116	1.84	654	4.06
TV05-Z	3.2	77	1.22	390	2.42
Data			77		175
TV03-E	3.3	9	0.57	121	0.78
TV03-N	3.3	40	2.65	140	0.91
TV03-Z	3.3	23	1.56	739	4.80
Data			29		168
TV10, TV14-E	8; 6	6	0.06	180	0.79
TV10, TV14-N	8; 6	255	2.83	92	0.41
TV10, TV14-Z	8; 6	7	0.08	1235	5.42
Data			104		242
TV08-E	10	46	0.41	283	1.70
TV08-N	10	126	1.11	308	1.84
TV08-Z	10	64	0.56	44	0.26
Data			127		181
TV13, TGYT-E	12.1	312	0.86	595	1.21
TV13, TGYT-N	12.1	131	0.36	401	0.81
TV13, TGYT-Z	12.1	390	1.08	615	1.25
Data			376		506

data-model fit (East, North and Up components of motion) for the entire observation period (1998–2005), while Table 5 summarizes the data and model fits of all GPS stations for the deformation episodes in 1998–2001 and 2004–2005. Model fits to the data during the first inflationary period (1998–2001) show small errors for the Volcano Island stations and the caldera wall stations. However, data-model fits for the second inflationary period (2004–2005) show slightly worse fits than the 1998–2001 period (Table 5). In particular, the stations near the summit (e.g., TV12, TV01, TV05) have larger misfits in the North and Vertical components for the later period, possibly resulting from localized sources of deformation (near the hydrothermal source reported in Zlotnicki et al., 2009).

5. Discussion

As shown by our pressurization experiments in step 2, the models using the purely elastic shell and the viscoelastic shell models can both produce comparable fits with the deformation values for both the L1 data and dual frequency data. Thus, without any *a priori* constraints, the forward estimation process is highly non-unique, providing numerous solutions to the problem. We can, however, use this comparison as a benchmark to compare the behavior of a rheologically complex model with the simple elastic model. We note that the magnitude and timing of deformation of predicted deformation associated with the viscoelastic shell model shows considerable differences with the instantaneous surface response produced by the elastic model.

The elastic models require that all inflation and deflation events are associated with coeval magmatic intrusion and withdrawal; in contrast, the viscoelastic structure offers the possibility to explain some of the deformation signals by time-delayed relaxation of the crust surrounding the magma body. Thus, when simple isotropic homogeneous elastic models are used, these delayed deformation signals associated with earlier pressure pulses could be mistaken for a later, distinct phases of magmatic influx. Assuming that the frequency and duration of these inflation–deflation cycles might result from intrinsic properties of the crust, they might be used as a constraint on crustal rheology. Thus, the observed periods of deformation at Taal (which is at most 270 d or less between successive periods) suggests lower material viscosities as compared to cycles associated with rhyolites (which have significantly longer relaxation times on the order of ~2300 d). Although the high-viscosity experiments provide insights on how the volcanic system would behave in a highly felsic environment (given that southwestern Luzon has experienced both silicic and mafic eruptions), we believe that the low-viscosity VE model (i.e., corresponding to andesitic magma) may be more realistic for Taal, which represents the rock composition from recent eruptions of Taal Volcano based on petrologic studies (i.e., Miklius et al., 1991; Mukasa et al., 1994; Castillo and Newhall, 2004).

Given the large difference (about a factor of four) of the inferred source pressure estimates between the elastic and the viscoelastic models, our results demonstrate that the source pressure may be grossly overestimated using purely elastic parameters (see Fig. 9). In turn, the stresses associated with reservoir inflation (and deflation) may also be overestimated, resulting in computed stress changes that may be larger than the actual host rock strength (see discussion in Newman et al., 2001). While we cannot rule out that the pressurization dictated by an elastic source may be correct, considering the appropriate rock rheology provides an additional physical constraint toward the determination of a more realistic pressure source.

The inflationary and deflationary patterns at Taal Volcano occur at intervals of about five to nine months with uplift rates to as much as 220 mm yr^{-1}, more frequent and larger than those measured from rhyolitic systems such as Yellowstone and the Long Valley Caldera in the western United States (Newman et al., 2006; Chang et al., 2007). There, the uplift rates are slower, i.e., with ~70 mm yr^{-1} vertical motion measured by continuous GPS at Yellowstone in 2004–2006 (Chang et al., 2007), and ~100 mm yr^{-1} uplift at station CASA at Long Valley during 1997 to 1998 (Newman et al., 2006). However, the temporal patterns of deformation at Taal show slower changes than those associated with low-viscosity magmatic systems such as Kilauea, Hawaii, where many eruptive sequences show rapid deformation pulses that span several hours to a few days (Owen et al., 2000).

Regarding the possibility that hydrothermal fluids may be the cause of inflationary cycles at Taal, Bartel et al. (2003) proposed that magmatic source change is likely the plausible explanation for uplift during the 2000–2001 period since no apparent increase in surficial (or shallow) hydrothermal activity was observed. However in early 2005 shallow hydrothermal sources may have affected the deformation signals of stations located near the summit, i.e., the northeast quadrant of Crater Lake, as strong thermal transfers and degassing were observed using electromagnetic, geochemical and thermal surveys (Zlotnicki et al., 2009). This suggests that some of the deformation events at Taal might be similar in nature to those at Yellowstone, proposed to result from pressurized hydrothermal fluids trapped underneath impermeable rocks (Chang et al., 2007). The advantage of these hydrothermal pressurization models is that they provide a mechanism to explain the inflation–deflation sequences without relying on new magmatic intrusion and withdrawal for each event. However, compared to magmatic

sources, these hydrothermal sources tend to be very shallow in nature (i.e., depth < 2 km), with longer and gentler pulses, and they may occur in areas asymmetric to the volcano axis (Dvorak and Dzurisin, 1997; Esposito et al., 2010). While it is possible that hydrothermal signals may have affected deformation signals of near-summit stations at the NE flank of Taal's main crater (Zlotnicki et al., 2009), the spatially broader signal we capture appears to be more deeply sourced and thus predominantly magmatic in origin. While the data available cannot fully resolve the source of this deformation, the viscoelastic models presented for Taal offer an alternative mechanism, at least for the broader part of the deformation cycle—i.e., that deformation is due to temporally-varying relaxation of the shells surrounding the magma chamber.

We believe that the method applied carries implications for geodetic monitoring and interpretation at other volcanic systems. First, because the near-source zone surrounding magma bodies is subjected to high temperatures and modest lithostatic pressures, an assumption of purely elastic behavior is generally not tenable. Our experimental work at Taal suggests two important implications common to most volcanic systems: (1) Observed variations in surface deformation need not result directly from changes in magmatic volume, pressure, and rather, can be the result of time-varying rheologic response to changes in the magmatic system, and (2) the inferred changes from inversion in simple elastic media are likely to significantly overestimate the pressure sources producing observed deformation. Because the scale and geometry of rheologic variability undoubtedly varies significantly from volcano to volcano, these conclusions cannot be applied directly to infer pressure source histories at other volcanoes. But it does indicate that direct interpretations of pressure changes associated with inferred point sources from geodetic source inversions must be treated with caution. Because volume change is an inferred quantity based on both inferred pressure and elastic constants (e.g., Lisowski, 2006), inferences about volume may suffer from similar ambiguity. A specific implication of our findings is that deflation of a magmatic system can result not from withdrawal of magma, but from relaxation of the viscoelastic materials surrounding a magma body. The viscoelastic models in our studies provide an additional physical constraint (i.e., realistic rock rheology) in determining accurate pressurization trends. This approach, when used in combination with denser geodetic datasets and more sophisticated finite element models that incorporate thermal effects, gravitation and lithostatic stresses (e.g., Grosfils, 2007; Gregg et al., 2012), may provide better insights on the time-dependent nature of magma chamber pressurization and its implications to reservoir wall rupture and eruptive processes.

6. Conclusions

We invert geodetic data to locate the magmatic source during the 2004–2005 inflationary period at Taal Volcano using point-source 'Mogi models' of volcanic pressurization. The inferred source location is comparable with that for the 2000 inflationary episode, showing an average source depth of ~5 km located near the center of Volcano Island. The similarity in the source position suggests a stable, non-migrating magmatic source for both of the two recent inflationary episodes. We then show that time-dependent surface deformation at Taal can be matched by different magma chamber pressurization trends, by factoring in variation in crustal rheology around the volcano. Specifically, we demonstrate that the inclusion of realistic viscoelastic models for the crust surrounding the volcano significantly reduces the required source pressure and introduces time-varying deformation signals that result from viscous response of the crust. Thus the relaxation of the crust beneath Taal Volcano can produce prolonged deformation signals that could be misinterpreted as new pressurization or depressurization trends, which in turn could contribute to inaccurate eruption forecasting. Overall, the viscoelastic models in our studies provide an additional physical constraint (i.e., realistic rock rheology) in determining accurate pressurization trends.

Acknowledgments

We acknowledge the major contribution from many individuals who contributed to the GPS field work, notably Tony Lowry and Beth Bartel from Indiana University, and Ernesto Corpuz, Agnes Aguilar, Julio Sabit and many others on the PHIVOLCS Volcano Monitoring team who contributed to the field effort. We also acknowledge the leadership of Chuck Meertens and the technical contributions of UNAVCO engineers Oivind Ruud, Spencer Reeder, Chuck Kurnik, Jay Sklar, and Karl Feaux, who helped design and install the continuous GPS networks at Taal. We thank Peter Cervelli (USGS) for the DisModel program, John Braun (UCAR) for his help on Bernese, Kaj Johnson, Heiju Hui, Ken Wohletz (for the K-Ware Magma program) and Altair Regienne Galgana for graphic illustrations. We thank Rocco Malservisi for constructive comments and thank Nicolas Fournier and Lionel Wilson for thorough reviews and editing, which improved the paper extensively. Some plots were made using GMT (Wessel and Smith, 1991). This research project was funded by the NSF grant EAR-0073992. This is LPI contribution No. 1765.

References

ABAQUS, Inc., 2003. Abaqus User's Manual, Version 6.4. Tech. Ref. Hibbit, Karlsson and Sorenson, Inc., Pawtucket, Rhode Island.

Aurelio, M., 2000. Shear partitioning in the Philippines: constraints from Philippine fault and global positioning system data. Island Arc 9, 584–597.

Barrier, E., Huchon, P., Aurelio, M., 1991. Philippine fault: a key for Philippine kinematics. Geology 19, 32–35.

Bartel, B., 2002. Magma dynamics at Taal Volcano, Philippines from continuous GPS measurements. Master's Thesis Department of Geological Sciences, Indiana University, Bloomington, Indiana (168 pp.).

Bartel, B.A., Hamburger, M.W., Meertens, C.M., Lowry, A.R., Corpuz, E., 2003. Dynamics of active magmatic and hydrothermal systems at Taal Volcano, Philippines, from continuous GPS measurements. J. Geophys. Res. 108 (B10), 2475. http://dx.doi.org/10.1029/2002JB002194.

Besana, G., Shibutani, T., Hirano, N., Ando, M., Bautista, B., Narag, I., Punongbayan, R., 1995. The shear wave velocity structure of the crust and uppermost mantle beneath Tagaytay, Philippines inferred from receiver function analysis. Geophys. Res. Lett. 22 (23), 3,143–3,146.

Bonafede, M., Dragoni, M., Quareni, F., 1986. Displacement and stress fields produced by a centre of dilatation and by a pressure source in a viscoelastic half-space: application to the study of ground deformation and seismic activity at Campi Flegrei, Italy. Geophys. J. R. Astron. Soc. 87, 455–485.

Castillo, P., Newhall, C., 2004. Geochemical constraints and possible subduction components in lavas of Mayon and Taal Volcanoes, Southern Luzon, Philippines. J. Petrol. 45 (6), 1,089–1,108.

Cervelli, P., Murray, M., Segall, P., Aoki, Y., Kato, T., 2001. Estimating source parameters from deformation data, with an application to the March 1997 earthquake swarm off the Izu Peninsula, Japan. J. Geophys. Res. 106 (B6), 11,217–11,237.

Chang, W., Smith, R., Wicks, C., Farrell, J., Puskas, C., 2007. Accelerated uplift and magmatic intrusion of the Yellowstone Caldera, Science, 2004 to 2006. Science 318 (5852), 952–956. http://dx.doi.org/10.1126/science.1146842.

Cole, J.W., Milner, D.M., Spinks, K.D., 2005. Calderas and caldera structures: a review. Earth-Sci. Rev. 69, 1–26.

Davis, P., 1986. Surface deformation due to inflation of an arbitrarily oriented triaxial ellipsoid cavity in an elastic half-space, with reference to Kilauea volcano, Hawaii. J. Geophys. Res. 80, 4,094–4,102.

Del Negro, C., Currenti, G., Scandura, D., 2009. Temperature-dependent viscoelastic modeling of ground deformation: application to Etna volcano during the 1993–1997 inflation period. Phys. Earth Planet. Inter. 172, 299–309.

Dieterich, J., Decker, R., 1975. Finite element modeling of surface deformation associated with volcanism. J. Geophys. Res. 80 (29), 4,094–4,102.

Dragoni, M., Magnanensi, C., 1989. Displacement and stress produced by a pressurized, spherical magma chamber, surrounded by a viscoelastic shell. Phys. Earth Planet. Inter. 56, 316–328.

Dvorak, J., Dzurisin, D., 1997. Volcano Geodesy: the search for magma reservoirs and the formation of eruptive vents. Rev. Geophys. 35 (3), 343–348.

Dzurisin, D., 2003. A comprehensive approach to monitoring volcano deformation as a window on the eruption cycle. Rev. Geophys. 41 (1), 1001. http://dx.doi.org/10.1029/2001 RG000107.

Esposito, A., Anzidei, M., Atzori, S., Devoti, R., Giordano, G., Pietrantonio, P., 2010. Modeling ground deformations of Panarea volcano hydrothermal/geothermal system (Aeolian Islands, Italy) from GPS data. Bull. Volcanol. 72, 609–621. http://dx.doi.org/10.1007/s00445-010-0346-y.

Fitch, T., 1972. Plate convergence, transcurrent faults, and internal deformation adjacent to Southeast Asia and the western Pacific. J. Geophys. Res. 77 (23), 4,432–4,460.
Förster, H., Oles, D., Knittel, U., Defant, M., Torres, R., 1990. The Macolod Corridor: a rift crossing the Philippine island arc. Tectonophysics 183, 265–271.
Galgana, G., Hamburger, M., McCaffrey, R., Corpuz, E., Chen, Q., 2007. Analysis of crustal deformation of Luzon Island, Philippines using geodetic observations and earthquake focal mechanisms. Tectonophysics 432, 63–87.
Gregg, P.M., de Silva, S.L., Grosfils, E.B., Parmigiani, J.P., 2012. Catastrophic caldera-forming eruptions: thermomechanics and implications for eruption triggering and maximum caldera dimensions on Earth. J. Volcanol. Geotherm. Res. 241, 1–12.
Grosfils, E.B., 2007. Magma reservoir failure on the terrestrial planets: assessing the importance of gravitational loading in simple elastic models. J. Volcanol. Geotherm. Res. 166 (2), 47–75.
Hibbit, Karlson, Sorenson, Inc., 1998. ABAQUS User's Manual, Version 5.8. Hibbit, Karlson, Sorenson, Inc., Pawtucket, Rhode Island.
Hugentobler, U., Schaer, S., Fridez, P. (Eds.), 2001. Bernese GPS Software Version 4.2. Astronomical Institute, University of Berne, Berne, Switzerland.
Ivins, E., 2000. Correction to "transient creep of a composite lower crust: 2. polymineralic basis for rapidly evolving post-seismic deformation modes". J. Geophys. Res. 105, 3,229–3,232.
Lisowski, M., 2006. Analytical volcano deformation source models. In: Dzurisin (Ed.), Volcano Deformation. Springer, Berlin Heidelberg, pp. 279–304.
Lowry, A., Hamburger, M., Meertens, C., Ramos, E., 2001. GPS monitoring of crustal deformation at Taal Volcano, Philippines. J. Volcanol. Geotherm. Res. 105, 25–47.
Manconi, A., Walter, T., Amelung, F., 2007. Effects of mechanical layering on volcano deformation. Geophys. J. Int. 170 (2), 952–958.
Manconi, A., Walter, T., Manzo, M., Zeni, G., Tizzani, P., Sansosti, E., Lanari, R., 2010. On the effects of 3-D mechanical heterogeneities at Campi Flegrei caldera, southern Italy. J. Geophys. Res. 115, B08405. http://dx.doi.org/10.1029/2009JB007099.
Masters, T., Shearer, P., 1995. Seismic models of the earth: elastic and anelastic. In: Ahrens, T.J. (Ed.), Global Earth Physics: A Handbook of Physical Constants, AGU Reference Shelf, vol. 1. American Geophysical Union, Washington DC, pp. 88–103.
McBirney, A., Murase, T., 1984. Rheological properties of magma. Annu. Rev. Earth Planet. Sci. 12, 337–357.
McTigue, D., 1987. Elastic stress and deformation near a finite spherical magma body: resolution of the point source paradox. J. Geophys. Res. 92, 12,931–12,940.
Miklius, A., Flower, M., Huijsmans, J., Mukasa, S., Castillo, P., 1991. Geochemistry of lavas from Taal Volcano, Southwestern Luzon, Philippines: evidence for multiple magma supply systems and mantle source heterogeneity. J. Petrol. 32, 593–627.
Mogi, K., 1958. Relations between the eruptions of various volcanoes and the deformations of the ground surfaces around them. Bull. Earth Res. Inst. 36, 99–134.
Moore, J., Nakamura, K., Alcaraz, A., 1966. The 1965 eruption of Taal Volcano. Science 151 (3,713), 955–960.
Mukasa, S., Flower, M., Miklius, A., 1994. The Nd-, Sr- and Pb-isotopic character of lavas from Taal, Laguna de Bay and Arayat volcanoes, southwestern Luzon, Philippines: implications for arc magma petrogenesis. Tectonophysics 235 (1994), 205–221.
Newman, A., Dixon, T., Ofoegbu, G., Dixon, J., 2001. Geodetic and seismic constraints on recent activity at Long Valley Caldera, California: evidence for viscoelastic rheology. J. Volcanol. Geotherm. Res. 105, 183–206.
Newman, A., Dixon, T., Gourmelen, N., 2006. A four-dimensional viscoelastic deformation model for Long Valley Caldera, California, between 1995 and 2000. J. Volcanol. Geotherm. Res. 150, 244–269.
Ohkura, T., et al., 2001. GPS measurements in the Macolod Corridor, Philippines. J. Geol. Soc. Philipp. 56 (3,4), 97–104.
Oles, D., Förster, H., Torres, R., Punongbayan, R., 1991. Geological Map of the Macolod Corridor. The German Agency for Technical Cooperation, the German Research Society and the Philippine Institute of Volcanology and Seismology.
Owen, S., Segall, P., Lisowski, M., Miklius, A., Murray, M., Bevis, M., Foster, J., 2000. January 30, 1997 eruptive event on Kilauea Volcano, Hawaii, as monitored by continuous GPS. Geophys. Res. Lett. 27 (17), 2,757–2,760.
Press, W., Teukolsky, S., Vetterling, W., Flannery, B., 1992. Numerical Recipes in FORTRAN. Cambridge University Press, New York., NY USA.
Poland, M., Hamburger, M., Newman, A., 2006. The changing shapes of active volcanoes: History, evolution, and future challenges for volcano geodesy. J Volcanol. Geotherm. Res. 150 (1), 1–13.
Pubellier, M., Garcia, F., Loevenbruck, A., Chorowicz, J., 2000. Recent deformation at the junction between the North Luzon block and the Central Philippines from ERS-1 Images. Island Arc 9, 598–610.
Richet, P., Lejeune, A., Holtz, F., Roux, J., 1996. Water and the viscosity of andesite melts. Chem. Geol. 128, 185–197.
Roche, O., Druitt, T.H., Merle, O., 2000. Experimental study of caldera formation. J. Geophys. Res. 105 (B1), 395–416.
Rothacher, M., Mervart, L. (Eds.), 1996. Bernese GPS Software Version 4.0. Astronomical Institute University of Berne, Berne, Switzerland.
Shaw, H.R., 1972. Viscosities of magmatic silicate liquids: an empirical method of prediction. Am. J. Sci. 272, 870–893.
Thibault, C.A., 1999. GPS measurements of crustal deformation in the northern Philippine Island Arc. M.S. thesis Dept. of Geological Sciences, Indiana University, Bloomington, IN (47 pp.).
Tiampo, K., Rundle, J., Fernandez, J., Langbein, J., 2000. Spherical and ellipsoidal volcanic sources at Long Valley Caldera, California, using a genetic algorithm inversion technique. J. Volcanol. Geotherm. Res. 102, 189–206.
Torres, R., Self, S., Punongbayan, R., 1995. Attention focuses on Taal: decade volcano of the Philippines. EOS Trans. AGU 76, 246–248.
Trasatti, E., Giunchi, C., Bonafede, M., 2003. Effects of topography and rheological layering on ground deformation in volcanic regions. J. Volcanol. Geotherm. Res. 122, 89–110.
Trasatti, E., Giunchi, C., Bonafede, M., 2005. Structural and rheological constraints on source depth and overpressure estimates at the Camp Flegrei caldera, Italy. J. Volcanol. Geotherm. Res. 144, 105–118.
Vogel, T., Flood, T., Patino, L., Wilmot, M., Maximo, R., Arpa, C., Arcilla, C., Stimac, J., 2006. Geochemistry of silicic magmas in the Macolod Corridor, Philippines: evidence of distinct, mantle-derived, crustal sources for silicic magma. Contrib. Mineral. Petrol. 151, 267–281.
Wessel, P., Smith, W., 1991. Free software helps map and display data. EOS Trans. AGU 72, 441.
Wohletz, K., 1999. Magma: calculates IUGS volcanic rock classification, densities, and viscosities. Los Alamos National Laboratory computer code LA-CC 99-28.Los Alamos National Laboratory, New Mexico.
Wolfe, J., Self, S., 1982. Structural lineaments and Neogene volcanism in Southwestern Luzon. The Tectonic and Geologic Evolution of Southeast Asian Seas and Islands, Part 2. The AGU Geophysical Monograph Series, 27, pp. 157–172.
Yang, X., Davis, P., Dietrich, J., 1988. Deformation from inflation of a dipping finite prolate spheroid in an elastic half-space as a model for volcanic stressing. J. Geophys. Res. 93 (B5), 4,249–4,257.
Zlotnicki, J., Sasai, Y., Toutain, J., Villacorte, E., Bernard, A., Sabit, J., Gordon, J., Corpuz, E., Harada, M., Punongbayan, J., Hase, H., Nagao, T., 2009. Combined electromagnetic, geochemical, and thermal surveys of Taal volcano (Philippines) during the period 2005–2006. Bull. Volcanol. 71 (1), 29–47.